Electrical Engineering (2024) 106:7509–7529
https://doi.org/10.1007/s00202-024-02449-x

ORIGINAL PAPER

A novel protection scheme for transmission lines connected to solar photovoltaic and wind turbine farms using fuzzy logic systems and bagged ensemble learning

Gotte Vikram Raju[1] · **Nandiraju Venkata Srikanth**[1]

Received: 28 January 2024 / Accepted: 26 April 2024 / Published online: 20 May 2024

Abstract
The integration of renewable energy sources (RESs), such as solar and wind power, into power systems presents unique challenges for transmission line protection. Traditional distance protection schemes may not be adequately sensitive or adaptable to the dynamic characteristics of RES-connected lines. To address these challenges, this paper proposes an intelligent novel protection scheme that combines fuzzy logic system for fault detection/classification with regression-based bagged ensemble learning for fault location estimation. The proposed scheme utilizes voltage signals of the bus connected to renewable energy sources processed with discrete Fourier transform (DFT) to extract relevant features for fault diagnosis. A Mamdani-based fuzzy inference system is implemented to analyze the DFT-extracted features and make decisions regarding fault occurrence and type. A bagged ensemble learning approach, incorporating multiple regression trees, is employed to accurately estimate the fault location along the transmission line. The performance and efficacy of the proposed protection scheme are verified through extensive MATLAB/SIMULINK simulations on the transmission line model integrated with renewable energy sources (solar and wind) considering the variations in different fault parameters with different solar irradiations and wind speeds. The results demonstrate that the scheme effectively detects and classifies various fault types in one cycle time, even under dynamic RES generation conditions. The proposed scheme achieved 99.56% accuracy in fault detection/classification confirming its reliable operation. Further, the proposed fault location estimation approach approximates the fault location within ± 5% error band, and the Chi-square test is performed to assess its reliability.

Keywords Ensemble learning · Fault detection/classification · Fault location · Fuzzy inference · Line protection · Renewable energy · Solar photovoltaic · Wind farm

Abbreviations

AFL	Actual fault location
AI	Artificial intelligence
ANN	Artificial neural network
ANFIS	Artificial neuro-fuzzy inference system
DFIG	Doubly fed induction generator
DFT	Discrete Fourier transform
DWT	Discrete wavelet transform
EFL	Estimated fault location
FD	Fault detection
FDC	Fault detection and classification
FIA	Fault inception angle
FIS	Fuzzy inference system
FLE	Fault location estimation
GPR	Gaussian process regression
GSC	Grid side converter
MODWT	Maximal overlap discrete wavelet transform
MPPT	Maximum power point tracking
P&O	Perturb and observe
PLL	Phase locked loop
PSO	Particle swarm optimization
PV	Photovoltaic
PWM	Pulse width modulation
RES	Renewable energy sources
RMS	Root-mean-square
RSC	Rotor side converter
SVM	Support vector machine
VSI	Voltage source inverter

✉ Gotte Vikram Raju
gottevr@student.nitw.ac.in

[1] Department of Electrical Engineering, National Institute of Technology, Warangal, India

1 Introduction

The global electrical energy demand is steadily increasing, driven by population growth, urbanization, and technological advancements. This escalating demand necessitates a sustainable energy for the future. The growing demand must be met besides addressing the challenge of climate change. To reduce the carbon emissions from conventional sources, nations across the globe are rapidly shifting towards renewable energy sources like solar and wind rather than fossil fuels for power generation. The integration of these inherently variable and geographically dispersed sources into the existing power grid poses significant challenges, especially in transmission line protection. Due to terrestrial and environmental conditions, renewable energy generation is not possible at all locations. The generated renewable power is to be transmitted to the load centres wherever it is required. The regional disparities in generation as well as demand necessitate the use of transmission lines.

The settings of conventional distance protection schemes are developed assuming the grid is solely supplied by the synchronous generators. Upon integration of renewables, the intermittent nature of renewable power sources creates problems to the distance relay operation that relies on the positive sequence components of voltage and current signals. The relay may issue false trips and experience underreach or overreach problems depending on the system operating conditions. Further, the faulty phase identification gets complicated due to the partial cancellation of positive and zero sequence components of currents during faults resulting in reduced fault currents than the healthy phase currents, i.e. accounted for the control mechanisms of the voltage source converters associated with the RES [1, 2]. A few latest papers were reviewed regarding the protection of transmission lines connected to RES.

Several authors have proposed different protection schemes to identify the faults on transmission lines connected to renewable energy sources which include modified distance protection, differential protection, pilot protection, and training-based artificial intelligent schemes. The pilot protection scheme utilizing currents at both ends of the line with a dynamic time warping algorithm reported in [3] is only for balanced faults and the pilot protection scheme implemented in [4] requires synchronized voltage and current data for fault impedance calculation using short line and distributed line models for wind power integrated transmission lines. Similarly, a modified fast distance relaying scheme utilizing the short line (R-L model) and Bergeron model of transmission line [5] and a modified polygonal distance protection for improved zone-1 performance [6] are proposed for wind farm connected transmission lines. Also, modified distance protection in [7] utilizing local voltage and current information for calculating line impedance and phase angle of fault impedance, differential protection in [8] utilizing signed correlation and fault index comparison to detect faults with the help of phase currents at both ends of the line, directional protection based on high frequency in [9] with the help of two independent relays processing voltage and current information available at ends of the line locally, and distance protection schemes employing least squares estimation [10] and multiple signal classification algorithm [11] to extract frequency components of voltage and current near to fundamental frequency are proposed by different authors to detect faults on the transmission lines connected to wind farms. Distance protection schemes for transmission lines connected to solar photovoltaic (PV) systems were also reported, viz. distance protection based on positive sequence network [12, 13] utilizing either PV side or grid side voltage and current information, and improved/modified distance protection based on fault impedance calculation in [14, 15] either utilizing synchronized/unsynchronized voltage and current data. Artificial intelligence-based protection schemes were also reported for the transmission lines connected to renewable energy sources. An enhanced distance protection with the help of support vector machine-based regression [16] for PV connected lines, ANFIS-based fault detection only for wind farm connected lines [17], fault detection/classification technique for wind farm connected lines using transient monitoring index with support vector machine in [18] and in [19] maximal overlap discrete wavelet transform with ANN for symmetrical fault detection only, and the intelligent protection methods [20, 21] for FACTS compensated line connected to wind farm with deep convolution neural network using variational mode decomposition and random forest classifier using intrinsic time scale decomposition are reported in the literature. Further, PSO optimized thresholds for adaptive differential protection of transmission lines connected to wind power systems are presented in [22, 23].

The protection schemes reported in most of the above-mentioned literature are hectic mathematical analysis-based distance/pilot/differential protection schemes which either require single/double end synchronized/unsynchronized current and/or voltage data for the protection task. On the other hand, the AI-based protection methods are reported which require massive datasets towards training the AI protection modules for fault detection/classification considering different operating scenarios of the system. Further, some protection schemes are implemented for the detection of symmetrical or balanced faults only.

This paper presents an intelligent novel protection scheme with a fuzzy logic system to identify and classify the short circuit faults of the transmission line connected to RES (solar and wind power sources). The voltage signals of the bus connected to renewable energy sources are pre-processed with DFT are the inputs to the proposed Mamdani based fuzzy inference system for fault detection/classification. A bagged

ensemble learning approach with regression decision trees is proposed for fault location estimation using the DFT processed voltage signals. The remaining paper is structured as follows: Sect. 2 presents the considered power system model details, Sect. 3 presents the feature extraction method and proposed protection scheme implemented, results and discussion are dealt in Sect. 4, and lastly conclusion in Sect. 5.

The key points of the proposed protection method are:

- The proposed scheme of protection approach with FIS demonstrates robust performance in identifying and classifying various fault types, even under variable generation conditions of the RES connected to lines.
- This scheme achieved an accuracy of 99.56% in fault detection and classification utilizing only single end voltage data that eliminates the use of communication link. Hence no communication latency.
- The FIS-based protection scheme is simple to implement and does not require any training for protection purposes.
- The bagged ensemble approach effectively reduces the estimation errors, ensuring a better approximation of the fault location that facilitates swift repair and restoration, minimizing downtime and enhancing grid resilience.
- The proposed approach demonstrates the potential of combining fuzzy logic, ensemble learning, and signal processing techniques for developing intelligent protection systems adaptable to modern power grids.

2 Details of power system model

In the present work, a 200 km length transmission line (400 kV and 50 Hz) connected to RES is considered. Figure 1 depicts the single-line schematic representation of the transmission system model with RES blocks and block representation of the protection scheme proposed. The represented power transmission system is modelled and simulated utilizing the MATLAB/Simulink platform. A three-phase power source represented with Thevenin's equivalent having 1.25 GVA short circuit capacity, and 10 X/R ratio is connected to one end of the line at Bus B3 represents the 400 kV, 50 Hz grid. The RES are connected at the other end of the line at Bus B1. The solar and wind powers of each 50 MW are integrated into the power system through the transmission line. The MATLAB components, viz. distributed parameters line block based on Bergeron's line model and three-phase fault breakers are used to simulate the transmission line having shunt capacitance effect and various fault types, respectively. The voltage samples collected at Bus B1 are utilized for the proposed protection technique. The parameters of the transmission line are given in Appendix I.

The solar photovoltaic (PV) power plant rated with 50 MW power consists of PV module, DC-DC boost converter, and voltage source inverter with a step-up transformer. A schematic representation of the solar power plant is shown in Fig. 2. An aggregate model of the 50 MW solar power plant is developed in MATLAB/Simulink that constitutes 50 number of solar PV parallel arrays each of 1 MW rated power. Each array consists of 205 number of parallel strings and each string has 14 number of series connected modules. The solar PV power plant data and the specifications of the PV module are given in Appendix II. The DC-DC boost converter is used to boost the PV voltage and extract the maximum power from the PV plant with perturb and observe maximum power point tracking algorithm. The 2-level three-phase voltage source inverter (VSI) and step-up transformer are used to interface/integrate the power of the PV plant into the power system. The block schematic of the inverter control is shown in Fig. 3. For further details on the design aspects related to the PV system, interested readers can refer to [24, 25].

The wind power is generated using the doubly fed induction generators (DFIG). Figure 4 presents the schematic representation of the DFIG-based wind farm. An aggregate model of the 50 MW wind power farm is developed in MATLAB/Simulink. The DFIG-based wind farm rated with 50 MW power consists of 33 number of wind turbine generators each of 1.5 MW rated power. The DFIG-based wind farm data is given in Appendix III. The wind turbine system, wound rotor induction generator, back-to-back converters (grid side converter (GSC) and rotor side converter (RSC)) with its associated control system, and the step-up transformer constitute the wind power farm. The power generated by wind farm is fed to the power system through the step-up transformer where the stator windings are directly connected to the transformer and rotor windings are connected through the back-to-back converters. The 2-level converters are used for GSC and RSC that maintain the dc link voltage and control the rotor currents, respectively. The block schematics of the converter control for RSC and GSC are shown in Figs. 5 and 6. For further details on the design aspects related to the wind power system, interested readers can refer to [24, 25].

3 Signal pre-processing and proposed scheme of protection

Generally, any digital scheme of protection involves majorly two stages. The first stage is the signal pre-processing to extract the relevant features useful for the protection task. The second stage is the implementation of the scheme of protection with the extracted features. In the present work, the simple and most widely applied discrete Fourier transform is employed as the signal processing technique and the scheme of protection is developed utilizing the fuzzy logic system

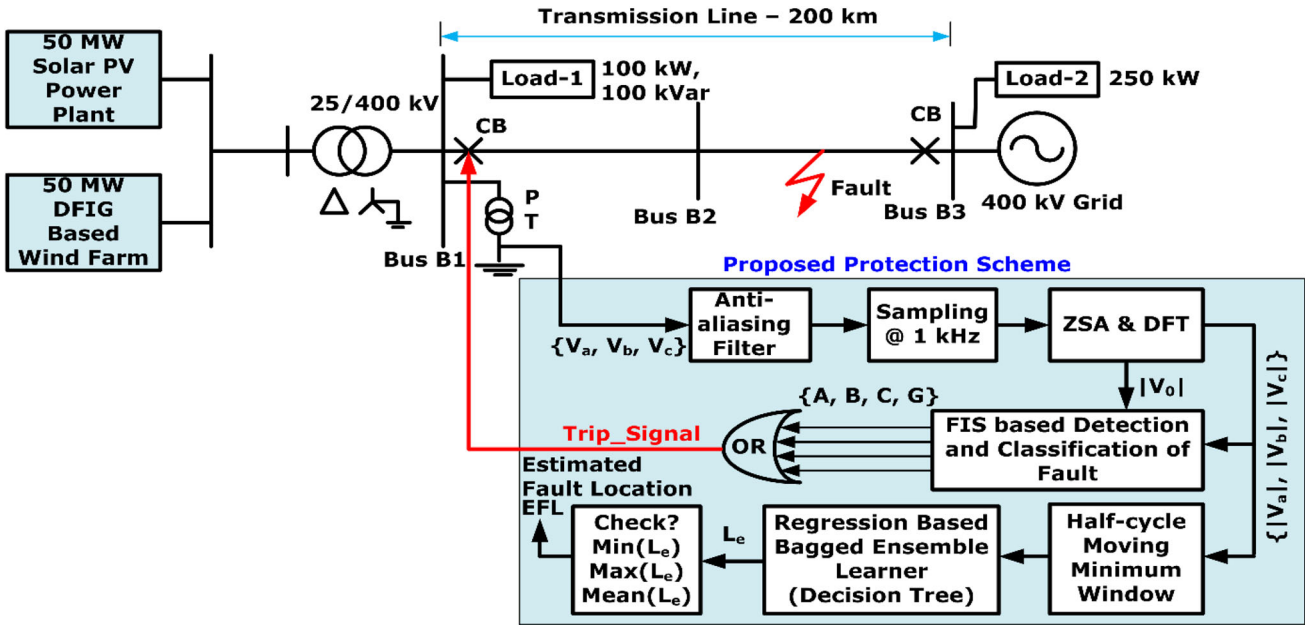

Fig. 1 Single-line schematic representation of power transmission system model along with block diagram of proposed protection method

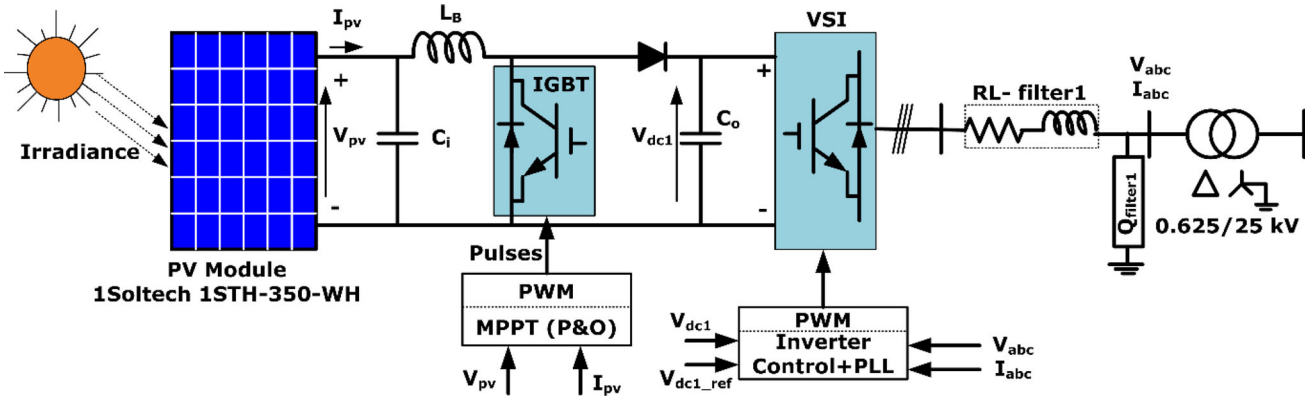

Fig. 2 Schematic representation of solar PV power source

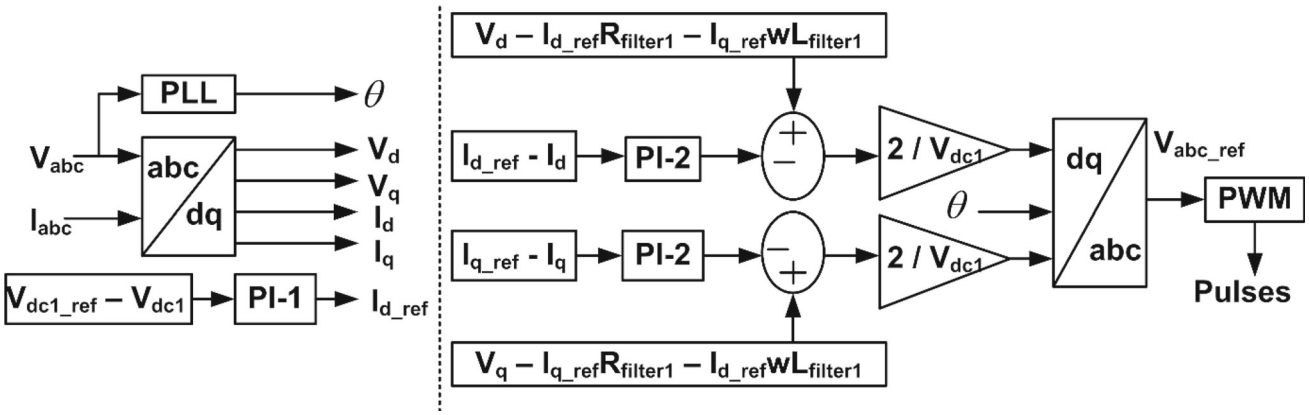

Fig. 3 Block schematic of inverter control

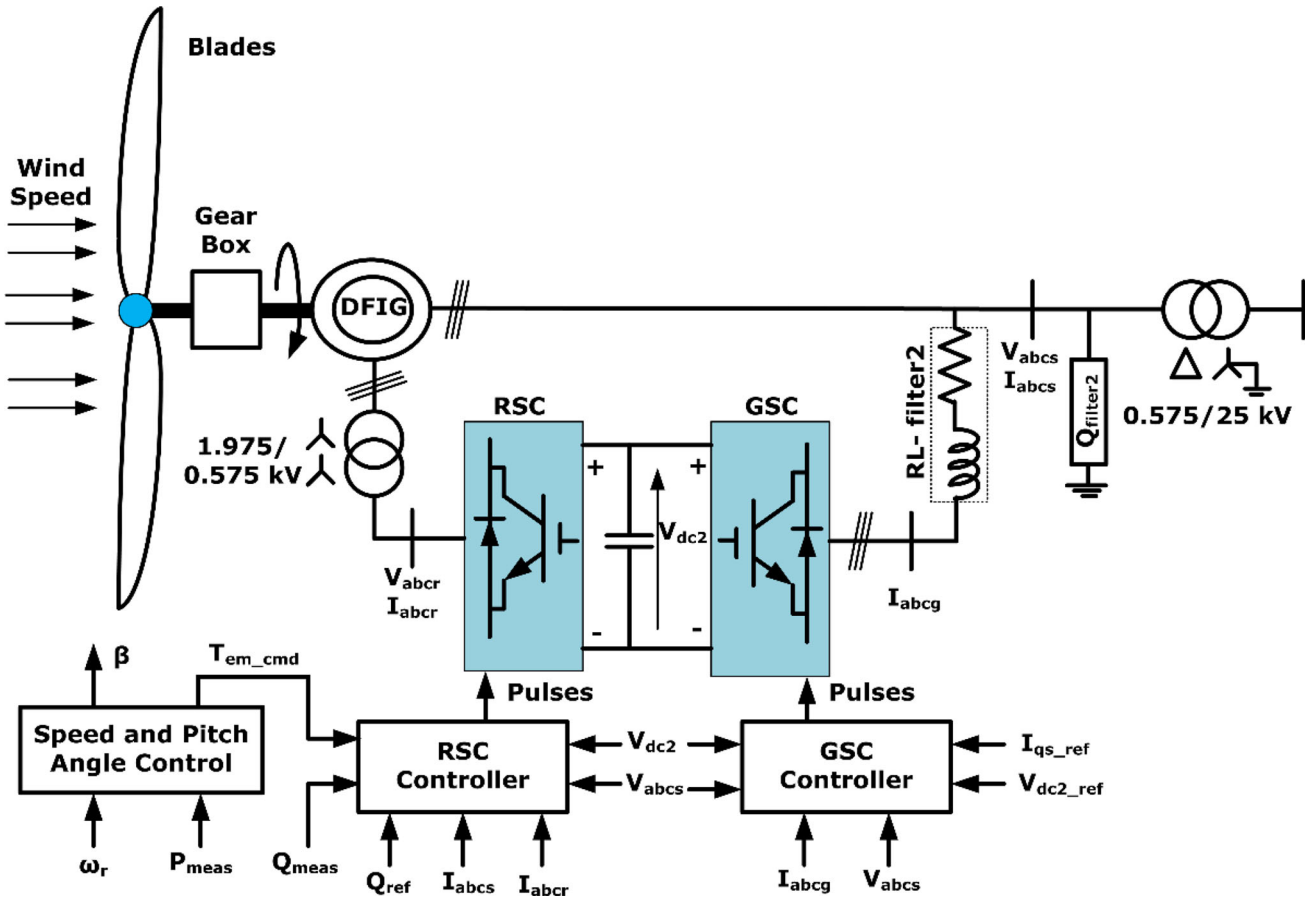

Fig. 4 Schematic representation of the DFIG-based wind farm

and ensemble learning approach with features retrieved by DFT.

3.1 DFT based feature extraction

The raw and unprocessed instantaneous fault information (either voltage or current data) captured at the relaying location are very transitory and oscillatory in nature due to which they cannot be directly used for the protection job. Hence, the raw fault data discretization and pre-processing with suitable digital signal processing technique is crucial. In the present study, the voltage samples collected at Bus B1 are only employed for the protection job because the amount of current injected into the grid may vary depending upon the intermittent operating conditions of the RES. But, irrespective of RES operating conditions, the voltage at Bus B1 is maintained almost invariable due to the control action of voltage source converters of RES. The initial stage of signal processing involves the filtering of three-phase voltage signals at Bus B1 using a low pass Butterworth anti-aliasing filter of second-order with 480 Hz cutoff frequency to ensure the removal of higher order voltage harmonics. According to the Nyquist sampling criterion, the filtered voltage signal is sampled with a 1 kHz sampling frequency. Using the discrete Fourier transform, the amplitude of the voltage signal's fundamental component is extracted/determined from the discrete voltage samples. Equation (1) gives $V_p(k)$, the discrete Fourier transform of $v_p(n)$ (discrete voltage samples) [26].

$$V_p(k) = \frac{1}{M}\sum_{n=0}^{M-1} v_p(n) e^{\frac{-j2\pi nk}{M}} \tag{1}$$

where $V_p(k)$ is the voltage phasor, $v_p(n)$ is a discretized voltage signal, p = *a*, *b*, and *c* phases, *n*, $k = 0, 1, 2, 3, \ldots, M\text{-}1$ are sample numbers, order of frequency stamps, and *M* is the number of samples per cycle. The zero-sequence voltage is determined utilizing MATLAB's sequence analyser to ensure the ground involvement in the fault loop of grounded faults. Therefore, the features extracted relevant to the scheme of protection are the magnitudes of fundamental component and zero-sequence component of three-phase voltage samples, viz. $\{|V_a|, |V_b|, |V_c|,$ and$|V_0|\}$.

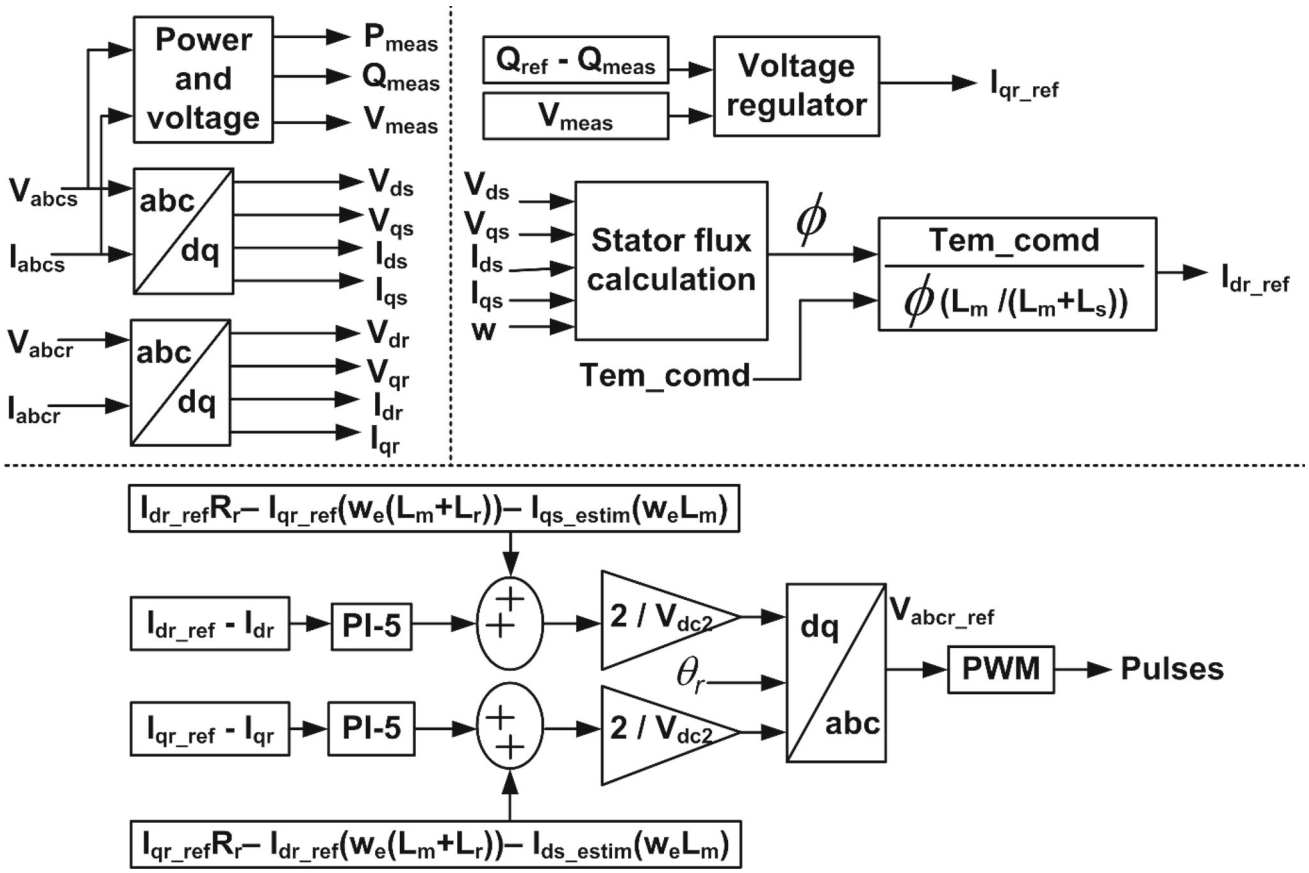

Fig. 5 Block schematic of RSC control

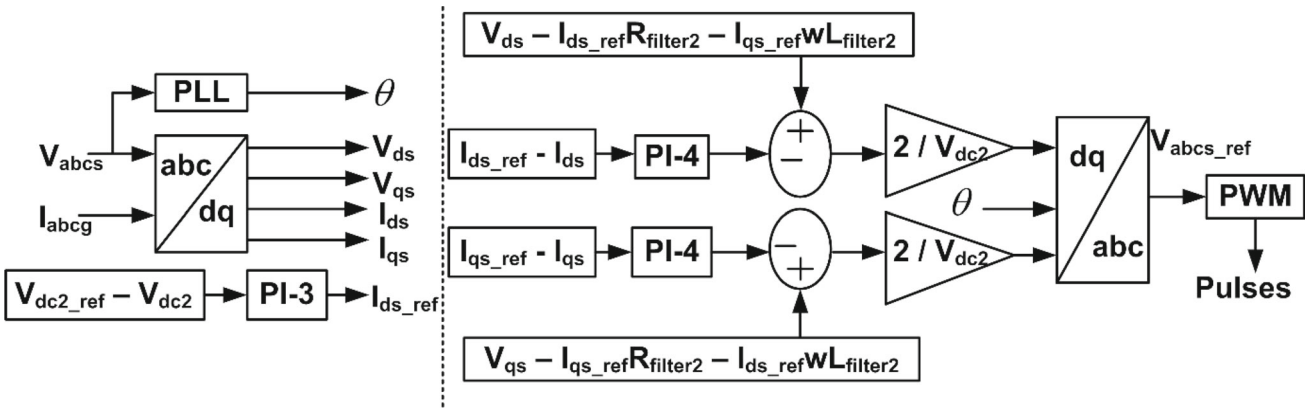

Fig. 6 Block schematic of GSC control

3.2 Proposed scheme of protection

The fuzzy logic system is used for the detection and classification of short circuit faults of the transmission line. Fuzzy logic systems are one of the AI techniques that are based on the fuzzy logic mathematical framework which works on vague/imprecise input data to produce precise output mimicking human like reasoning. These are simple, flexible, and have an easily implementable structure. They can solve nonlinear problems without intense computational effort regardless of the system's mathematical model. Fuzzy set theory forms the base for fuzzy logic concepts. Unlike the traditional binary logic where the possible outcomes are categorized as either completely true or false, i.e. 1 or 0, fuzzy logic introduces the concept of partial truthiness or falseness ranging its degree from 0 to 1 that embraces the ambiguity of real-world problems. These rule-based systems make decisions using the fuzzy logic idea. The execution of these

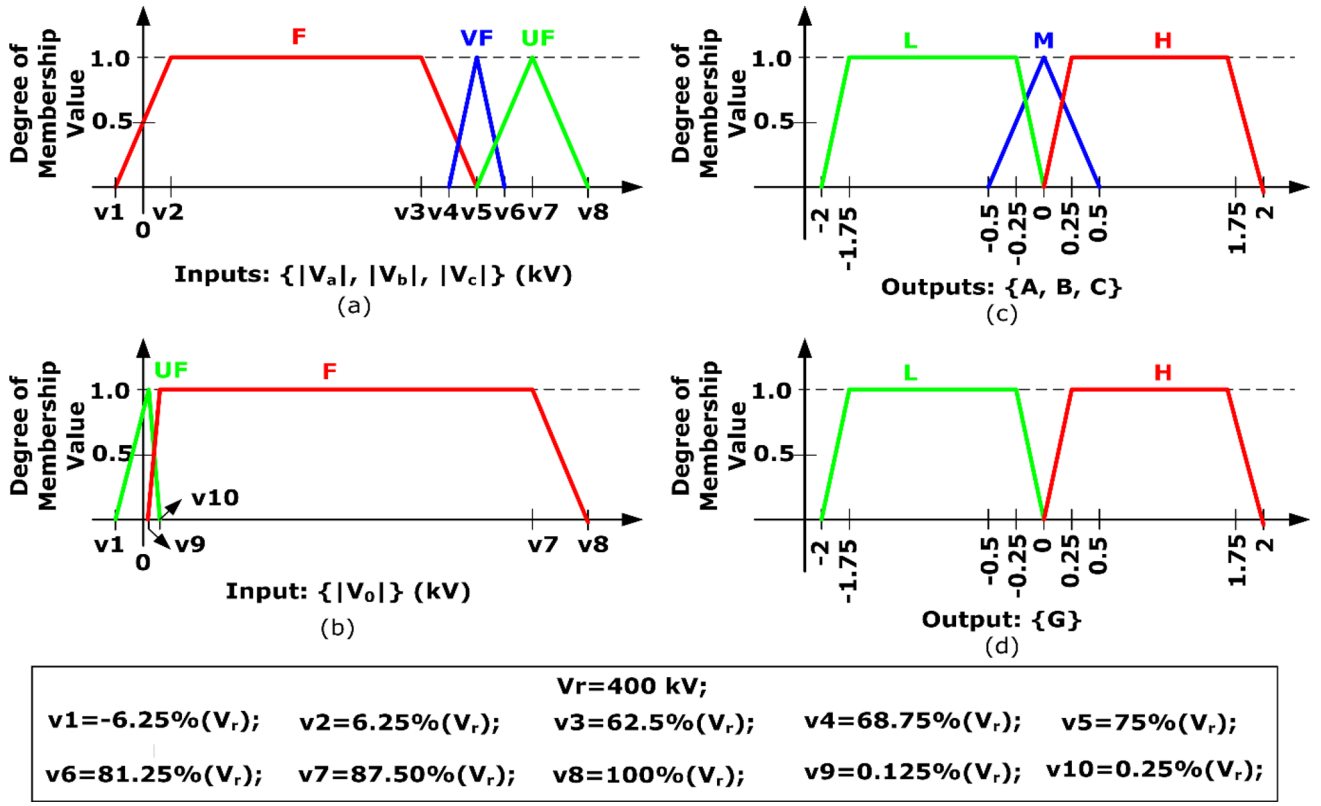

Fig. 7 Fuzzification of inputs and outputs

systems is based on a set of devised "if–then" fuzzy rules that establish conditional relationships mapping the input–output fuzzy sets represented by the membership functions. The execution involves processes like fuzzifying inputs and outputs, fuzzy inference processing, and defuzzification of outputs [27].

A single module of the Mamdani fuzzy inference system (FIS) is developed using MATLAB's Fuzzy Logic Toolbox to make decisions about the transmission line fault type and its occurrence. The FIS accepts four inputs *{*$|V_a|$, $|V_b|$, $|V_c|$, and$|V_0|$*}* and provides four outputs *{A, B, C,* and*G}* to identify and classify the faults. The inputs and outputs are organized into different fuzzy sets with the fuzzy linguistic variables labelled as *F (*fault*),* VF *(*verge of fault*),* and UF (unfault) for the inputs, and *L* (Low),*M* (Medium), and *H* (High) for the outputs. The fuzzy linguistic variables of the inputs and outputs are represented with the trapezoidal *(F, L,* and *H)* and triangular *(*VF, UF, and *M)* membership functions. Figure 7 depicts the graphical representation of the fuzzification of inputs and outputs.

The suggested protection scheme employs 23 fuzzy rules that are formulated with the input–output fuzzy linguistic variables to detect/classify the faults. Table 1 presents the formulated fuzzy rule base of the scheme with rule no. #1 as "If $|V_a|$ is UF and $|V_b|$ is UF and $|V_c|$ is UF then *A* is *L*, *B* is *L*, *C* is *L*". In a similar fashion, all other framed rules can be interpreted. The outputs *{A*, *B*, and *C}* are dedicated to detect the phase(s) is faulty or healthy represented with the output labels " + 1" or "−1", respectively. Similarly, the output *{G}* is engaged in the detection of ground for the grounded faults. The centroid method of defuzzification is applied to the aggregated fuzzy outputs to deliver a crisp value that signifies the fault severity. Whenever a fault is detected, the faulty phase output of the FIS module shows "High" with label " + 1" and for healthy phase the module output is "Low" with "−1". The OR operation is performed on the FIS outputs *{A, B,* and*C}* to issue the trip signal to the circuit breaker. The upper and lower limits of fault detection and classification are considered as + *1* and −1 to represent the faulty and healthy conditions of the line and to avoid any unnecessary relay operation for small voltage fluctuations that might be considered as faults. The overlapping region of membership functions 'VF' and *'F'* of inputs *{|Va|, |Vb|, and |Vc|}* take care of small voltage dips/drops where FIS outputs vary from *0* to + 1 depending on fault severity. If the voltage sag persists and drops further, the FIS outputs take a transition from *0* to + 1 depending on the abnormality severity. Similarly, the voltage fluctuations above the normal operating voltage are taken care of by the membership functions *'VF'* and *'UF'* of inputs *{|Va|, |Vb|, and |Vc|}* where FIS outputs

Table 1 Framed fuzzy rules

# Rule no.	Membership functions for								# Rule no.	Membership functions for							
	$\|V_a\|$	$\|V_b\|$	$\|V_c\|$	$\|V_0\|$	A	B	C	G		$\|V_a\|$	$\|V_b\|$	$\|V_c\|$	$\|V_0\|$	A	B	C	G
#1	*UF*	*UF*	*UF*	–	*L*	*L*	*L*	–	#13	*VF*	*VF*	*F*	–	*M*	*M*	*H*	–
#2	*VF*	*VF*	*VF*	–	*M*	*M*	*M*	–	#14	*UF*	*VF*	*F*	–	*L*	*M*	*H*	–
#3	*F*	*F*	*F*	–	*H*	*H*	*H*	–	#15	*VF*	*UF*	*F*	–	*M*	*L*	*H*	–
#4	*F*	*UF*	*UF*	–	*H*	*L*	*L*	–	#16	*F*	*F*	*UF*	–	*H*	*H*	*L*	–
#5	*F*	*VF*	*VF*	–	*H*	*M*	*M*	–	#17	*F*	*F*	*VF*	–	*H*	*H*	*M*	–
#6	*F*	*VF*	*UF*	–	*H*	*M*	*L*	–	#18	*UF*	*F*	*F*	–	*L*	*H*	*H*	–
#7	*F*	*UF*	*VF*	–	*H*	*L*	*M*	–	#19	*VF*	*F*	*F*	–	*M*	*H*	*H*	–
#8	*UF*	*F*	*UF*	–	*L*	*H*	*L*	–	#20	*F*	*UF*	*F*	–	*H*	*L*	*H*	–
#9	*VF*	*F*	*VF*	–	*M*	*H*	*M*	–	#21	*F*	*VF*	*F*	–	*H*	*M*	*H*	–
#10	*UF*	*F*	*VF*	–	*L*	*H*	*M*	–	#22	–	–	–	*UF*	–	–	–	*L*
#11	*VF*	*F*	*UF*	–	*M*	*H*	*L*	–	#23	–	–	–	*F*	–	–	–	*H*
#12	*UF*	*UF*	*F*	–	*L*	*L*	*H*	–									

vary from *0* to −1. If the system is healthy, the FIS outputs are −1 but when the voltage fluctuations rise the FIS outputs traverse from −1 to 0 depending on the abnormality condition. In this way, the proposed FIS based protection module provides a better decision on the fault and normal conditions with a transition of FIS outputs from −1 to + 1 instead of a sharp threshold. This setting improves the sensitivity and selectivity of the proposed protection scheme.

This work employs a regression based bagged ensemble learning approach with decision trees strategy for estimation/prediction of fault location. The ensemble learning approach is one of the machine learning techniques, i.e. used to improve the overall prediction accuracy and robustness of the model. An ensemble learner is one which combines the results of many learners to give a final output of high quality. In the bagged ensemble learning approach, the learners/models are independent of each other and are trained/processed parallelly on the training data set or subsets of training data that are obtained by sampling the initial training data set with replacement. Instead of single model training that may be prone to underfitting/overfitting due to data changes, the bagging ensemble process that trains multiple models avoids the overfitting issues making the system robust with good generalization performance. A pictorial representation of the bagged ensemble learner is shown in Fig. 8, where $D_{\mathrm{K,d}}$ is the original training data set of K rows (instances) and d columns (d-1 features/attributes and the last column represents the target data), $D^1{}_{\mathrm{K1,d}}$, $D^2{}_{\mathrm{K1,d}}$, $D^3{}_{\mathrm{K1,d}}$, …, $D^n{}_{\mathrm{K1,d}}$ are the subsets of training data, M_1, M_2, M_3, …, M_n are individual models/learners, Y_1,Y_2,Y_3, …, Y_n are the individual model outputs, and n is the number of learners in the ensemble. The Y is the final output of the ensemble. If the bagged ensemble is used for classification purpose,

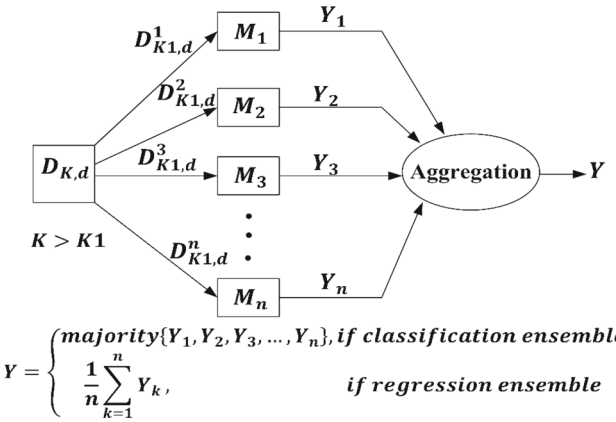

Fig. 8 Pictorial representation of bagged ensemble learner

then the final aggregated output is based on the majority voting method and if it is a regression ensemble then the final aggregated output is the average of all the individual outputs [28–30].

In the proposed protection method, an ensemble of decision trees (regression) is implemented. Decision trees are one of the paradigms of data mining that are based on non-parametric supervised learning algorithms and are capable of effectively predicting input feature and output target relationships. The fundamental principle of growing decision trees is to *'divide and conquer'* the training data by recursively splitting/partitioning the data optimally using *'if–then'* conditions until the desired stopping criterion is reached. Impurity based calculations are employed for optimal splitting of the data to get a pure node in classification trees whereas minimum mean squared error of prediction is used to define the purity of split in regression trees. A pictorial representation of the

$$D = \begin{bmatrix} f_1 & f_2 & . & . & f_d \\ & & a_{ij} & & \\ & & i = 1\ to\ N & & \\ & & j = 1\ to\ d & & \end{bmatrix} \quad Y = \begin{bmatrix} y_1 \\ y_2 \\ . \\ . \\ y_N \end{bmatrix} \quad S = \begin{bmatrix} S_1 & S_2 & . & . & S_d \\ & & s_{ij} & & \\ & & i = 1\ to\ N-1 & & \\ & & j = 1\ to\ d & & \end{bmatrix} \quad where\ S_j = \frac{a_{ij} + a_{(i+1)j}}{2}$$

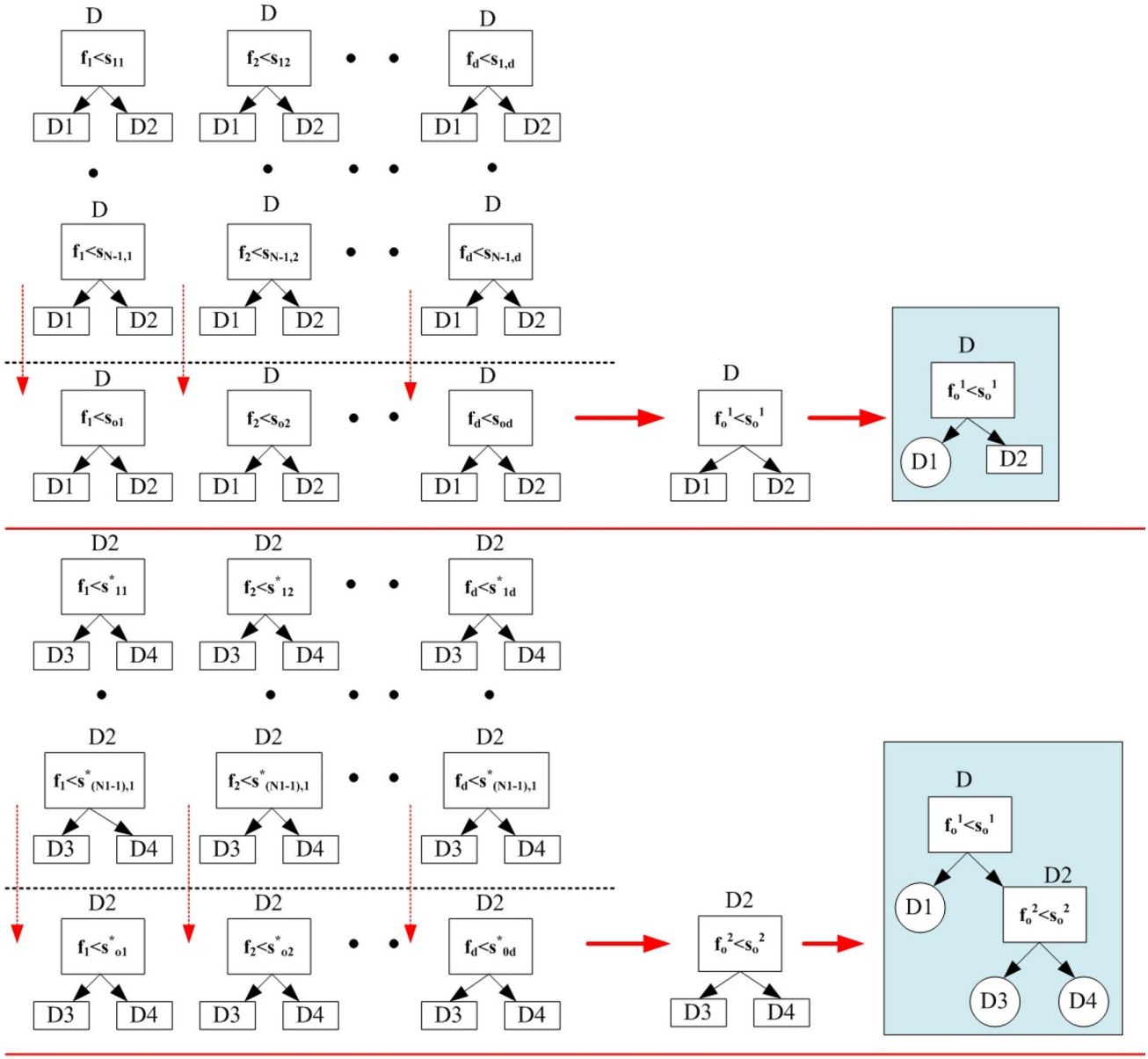

Fig. 9 Pictorial representation of decision tree growing

decision tree growing is shown in Fig. 9 where the training data D contains features/attributes $(f_1, f_2, \ldots, f_d)$ with N no. of instances, Y is the target data, and S is the potential splits obtained from D. The optimal splits and optimal features are derived from impurity-based calculations through the minimization of mean squared error of prediction. The process of splitting the data is continued until the pure nodes are attained or the maximum depth of the tree is reached [31–33]. In Fig. 9, the pure node is represented with a circle and the impure node is represented with a rectangle.

A bagged ensemble of 300 number of decision trees is implemented using regression learner in MATLAB to estimate the location of the fault. An extensive number of fault

Table 2 Fault parameters considered in the training data set

S. No.	Fault parameter	Variations
1	Fault resistance (Ω)	0.01 Ω, 50 Ω, and 100 Ω (3 no.)
2	Fault inception angle (°)	0° and 90° (2 no.)
3	Fault location (km)	3 km, 6 km, 9 km, …, 194 km, and 197 km (66 no.)
4	Fault types	10 (ABC, AB, BC, CA, ABG, BCG, CAG, AG, BG, and CG)

Therefore, total no. of fault cases considered = 3*2*66*10 = 3960 and 3—no fault case

simulations were conducted on the modelled system to generate the fault data for training the bagged ensemble learner. A total of 3960 different fault cases were simulated considering the variations in different fault parameters, viz. fault resistance, fault inception angle, fault location, and different fault types. Table 2 presents the details of fault parameters considered to generate the training data set. The size of the training data set is 39,630*4, where the first three columns represent the half-cycle moving minimum window of the inputs $\{|V_a|, |V_b|, \text{and } |V_c|\}$ and the last column represents the actual fault location (target). In the training data set, the actual fault location of no-fault cases is labelled as 400 km. The half-cycle post fault data (10 samples) is collected to construct the training data set. The bagged ensemble learner with different number of trees and minimum leaf sizes are trained on the generated data set through a series of pilot runs. The bagged ensemble learner with 300 number of trees and a minimum leaf size of one is found to be feasible. The estimated fault location (EFL) is derived from the minimum, maximum, and mean of the estimated location (L_e). Whenever a fault is detected (i.e. $L_e < 400$ km), then one cycle data of L_e is collected and the EFL is evaluated depending on the conditions given in Eq. (2) using the one cycle data. The training process took a time of 93.12 s to train the bagged ensemble model with the prediction metrics: root mean squared error of

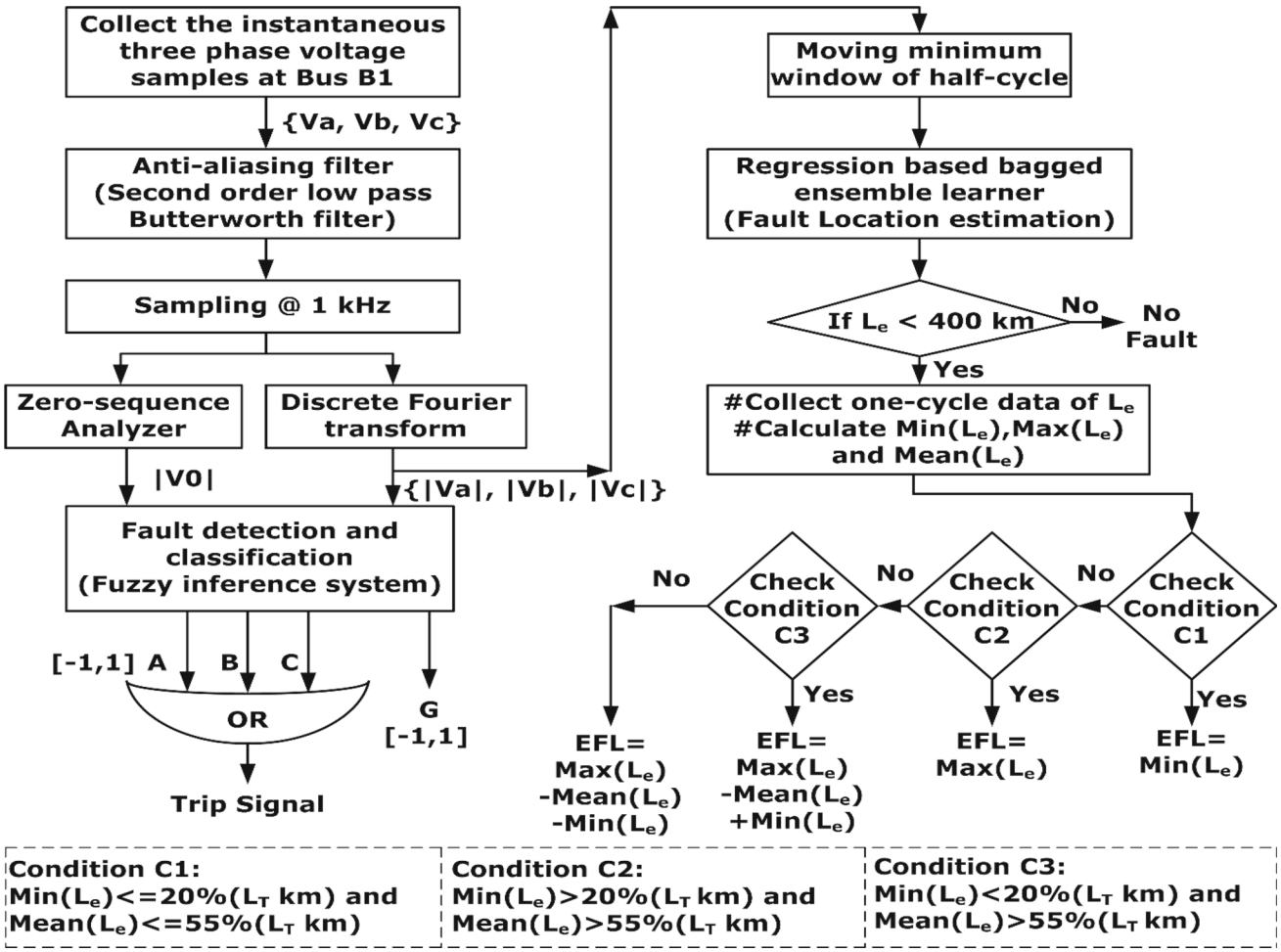

Fig. 10 Flowchart of the complete scheme of protection

0.996, mean squared error of 0.991 and mean absolute error of 0.719. All the simulations of the present work are carried out on the Intel® Core(TM) i5-10210U CPU @ 2.11 GHz processor with 8 GB RAM Windows 11 operating system. Figure 10 presents the flowchart of the complete scheme of the suggested protection method and its block diagram is shown in Fig. 1.

$$\mathrm{EFL} = \begin{cases} Min(L_e),\ if\ Min(L_e) \le 20\%(L_T)\ and\ Mean(L_e) \le 55\%(L_T) \\ \mathrm{Max}(L_e),\ \text{if}\ \mathrm{Min}(L_e) > 20\%(L_T)\ \text{and}\ \mathrm{Mean}(L_e) > 55\%(L_T) \\ \mathrm{Max}(L_e) - \mathrm{Mean}(L_e) + \mathrm{Min}(L_e),\ \text{if}\ \mathrm{Min}(L_e) < 20\%(L_T)\ \text{and}\ \mathrm{Mean}(L_e) > 55\%(L_T) \\ Max(L_e) - Mean(L_e) - Min(L_e),\ if\ Min(L_e) > 20\%(L_T)\ and\ Mean(L_e) < 55\%(L_T) \end{cases} \quad (2)$$

Here, L_T, L_e, and EFL are the total length of the transmission line, estimated location, and estimated fault location in km, respectively.

4 Results and discussion

The performance of the proposed scheme of protection is discussed in this section by carrying out extensive fault simulations on the simulated power system model. The suggested protection method utilizes FIS for detection/classification of fault and a regression based bagged ensemble approach for fault location estimation. The protection scheme's efficacy is evaluated for ten different types of short circuit faults simulated on the transmission line by varying different fault parameters (fault resistance, R_f (0–100 Ω), fault inception angle, ϕ, (0°–360°), and fault location, L_f (1–200 km)) with different solar irradiance and wind speed levels.

4.1 Performance evaluation of FIS module for detection and classification of faults

Short circuit faults are stochastic in nature and can occur at location on any phase(s) of the transmission line. To evaluate the performance of the FIS-based protection module different short circuit faults are simulated. An LG fault (AG) with fault resistance $R_f = 50\ \Omega$ and fault inception angle $\phi = 0°$ (time of fault, $T_f = 0.2$ s) is simulated at a fault location of 50 km from the Bus B1 with solar irradiance of 1000 W/m^2 and wind speed of 15 m/s. The three-phase voltage, current, power, and magnitude of voltage features $\{|V_a|, |V_b|, |V_c|,$ and $|V_0|\}$ measured at Bus B1 are depicted in Fig. 11 for the above-mentioned fault. Figure 11e presents the FIS based protection module outputs *{A, B, C, G}* representing the fault detection and classification (FDC). From the FIS outputs, it can be observed that until 0.2 s the output level of all the output labels is "−1" (healthy condition) and after the occurrence of the AG fault at 0.2 s the output level of outputs *A* and *G* is " + 1" (faulty condition) at 0.206 s indicates the instant of fault detection and its type. Hence, the proposed protection scheme clearly identifies the fault type and its occurrence with the FDC time as 6 ms (FDC time = 0.206–0.2 ms = 6 ms), i.e. less than one cycle time (20 ms). Further, the performance of the proposed scheme is evaluated for different fault types with solar irradiance of 1000 W/m^2 and wind speed of 15 m/s for variations in fault resistance (Table 3), fault inception angle (Table 4), and fault location (Table 5). The $L_f = 50$ km and $\phi = 0°$ are kept constant in Table 3, the $R_f = 50\ \Omega$ and $L_f =$ 105 km are kept constant in Table 4, and the $R_f = 20\ \Omega$ and $\phi = 0°$ are kept constant in Table 5 for the tabulated results.

Further, the performance of the proposed FIS protection module is evaluated for faults with different solar irradiance and wind speed levels. Figure 12 depicts the results of the proposed scheme for the LLG fault (ABG) with the following parameters: $L_f = 90$ km, $R_f = 80\ \Omega$, $T_f = 0.5$ s ($\phi = 0°$), solar irradiance = 500 W/m^2, and wind speed = 8 m/s. From Fig. 12d, it can be observed that the ABG fault is detected and classified within 7 ms after the inception of the fault. Similarly, Fig. 13 depicts the results of the proposed scheme for the LLL fault (ABC) with the following parameters: L_f = 150 km, $R_f = 30\ \Omega$, $T_f = 0.5$ s ($\phi = 0°$), solar irradiance = 1200 W/m^2, and wind speed = 20 m/s. The ABC fault is identified in 8 ms after the inception of the fault. Tables 6 and 7 showcase the performance of the proposed method under varying fault conditions. Table 6 presents results for solar irradiance of 500 W/m^2 and wind speed of 8 m/s, while Table 7 focuses on solar irradiance of 1200 W/m^2 and wind speed of 20 m/s. Both tables explore the impact of different fault types and variations in fault parameters. The results presented showcase the effectiveness of the proposed FIS protection module even under different operating conditions of the RES for varying transmission line fault conditions.

Further, the reliable operation of the proposed scheme of protection is assessed in terms of accuracy and dependability with the help of a confusion matrix. The accuracy and dependability are calculated using Eq. (3) and Eq. (4). The confusion matrix is developed for the fault cases that are described in Table 2 (3963 fault cases) and Table 10 (2400 fault cases). The number of true and detected fault cases is segregated into LG, LLG, LL, LLL, and NF fault types depicted in Table 8 are listed in the confusion matrix. The

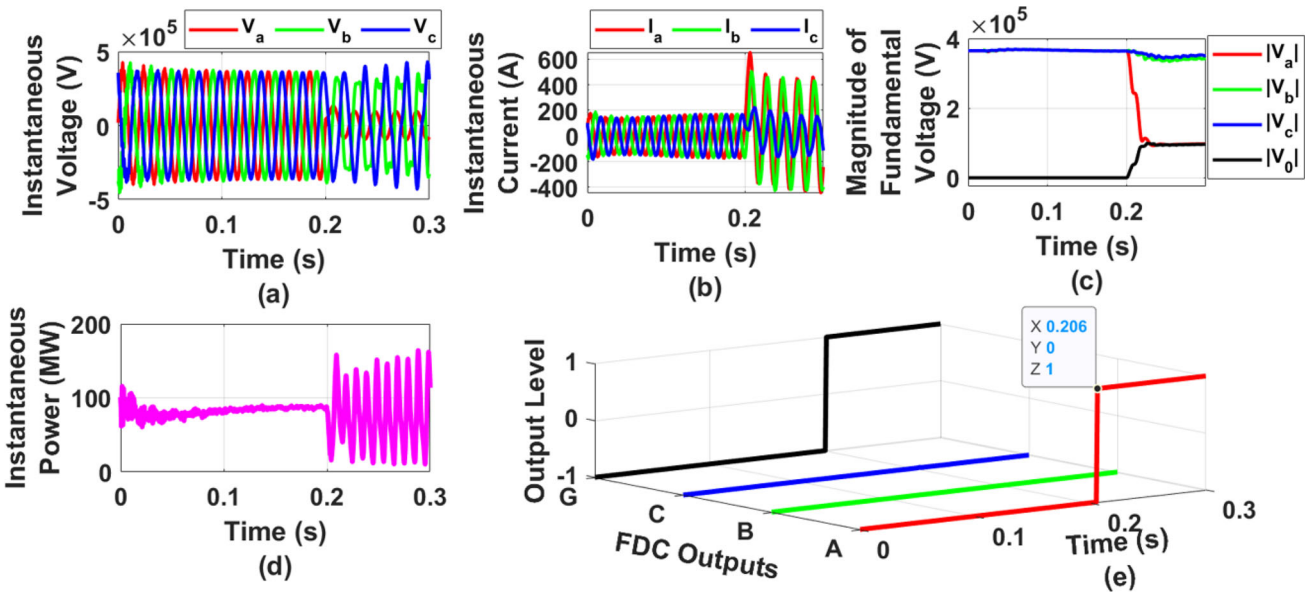

Fig. 11 AG fault with $R_f = 50\ \Omega$, $\phi = 0°$ ($T_f = 0.2$ s), $L_f = 50$ km, solar irradiance = 1000 W/m^2, and wind speed = 15 m/s. **a** and **b** Voltage and current waveforms at Bus B1, **c** Voltage magnitudes of fundamental component and zero-sequence component, **d** Three phase power from renewables, and **e** FDC outputs

Table 3 Performance results of the proposed FIS protection module for varying fault resistance

Solar irradiance = 1000 W/m^2 and wind speed = 15 m/s							$L_f = 50$ km and $\phi = 0°$ ($T_f = 0.2$ s)			
S. No.	Fault type	R_f (Ω)	FIS-based FDC outputs				FDC time (ms)			
			A	*B*	*C*	*G*	*A*	*B*	*C*	*G*
1	AG	0.01 Ω	1	− 1	− 1	1	5 ms	–	–	1 ms
2	BG	50 Ω	− 1	1	− 1	1	–	3 ms	–	1 ms
3	ABG	50 Ω	1	1	− 1	1	5 ms	3 ms	–	1 ms
4	BCG	100 Ω	− 1	1	1	1	–	3 ms	8 ms	1 ms
5	AB	5 Ω	1	1	− 1	− 1	6 ms	4 ms	–	–
6	ABC	10 Ω	1	1	1	− 1	6 ms	3 ms	8 ms	–

Table 4 Performance results of the proposed FIS protection module for varying fault inception angle (FIA)

Solar irradiance = 1000 W/m^2 and wind speed = 15 m/s							$R_f = 50\ \Omega$ and $L_f = 105$ km			
S. No.	Fault type	FIA (ϕ°) (T_f (s))	FIS-based FDC outputs				FDC time (ms)			
			A	*B*	*C*	*G*	*A*	*B*	*C*	*G*
1	AG	0° (0.2 s)	1	− 1	− 1	1	6 ms	–	–	2 ms
2	ABG	45° (0.2025s)	1	1	− 1	1	3.5 ms	8.5 ms	–	2.5 ms
3	AB	90° (0.205 s)	1	1	− 1	− 1	10 ms	8 ms	–	–
4	ABC	180° (0.21 s)	1	1	1	− 1	6 ms	3 ms	8 ms	–
5	BCG	270° (0.215 s)	− 1	1	1	− 1	–	8 ms	4 ms	1 ms

Table 5 Performance results of the proposed FIS protection module for varying fault location

Solar irradiance = 1000 W/m^2 and wind speed = 15 m/s							$R_f = 20\ \Omega$ and $\phi = 0°$ ($T_f = 0.2$ s)			
S. No.	Fault type	L_f (km)	FIS-based FDC outputs				FDC time (ms)			
			A	*B*	*C*	*G*	*A*	*B*	*C*	*G*
1	CG	5 km	− 1	− 1	1	1	–	–	7 ms	1 ms
2	ABG	50 km	1	1	− 1	1	6 ms	3 ms	–	1 ms
3	ABC	100 km	1	1	1	− 1	6 ms	3 ms	8 ms	–
4	BC	150 km	− 1	1	1	− 1	–	4 ms	9 ms	–
5	AG	197 km	1	− 1	− 1	1	5 ms	–	–	2 ms

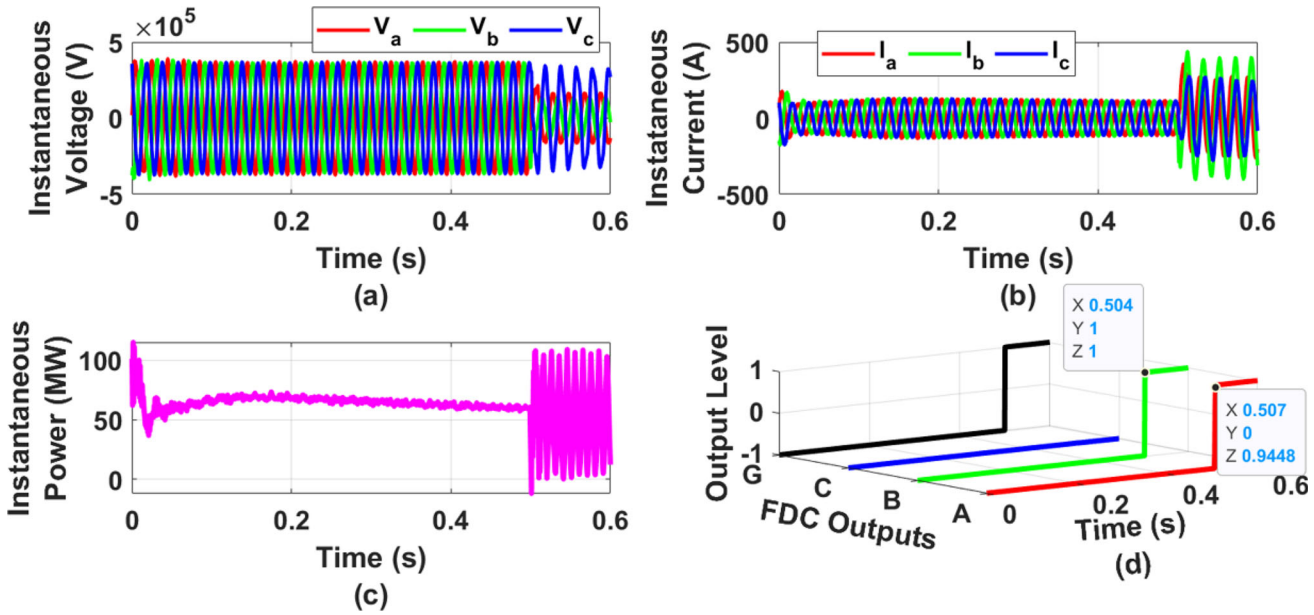

Fig. 12 ABG fault with $R_f = 80\ \Omega$, $\phi = 0°$ ($T_f = 0.5$ s), $L_f = 90$ km, solar irradiance = 500 W/m^2, and wind speed = 8 m/s. **a** and **b** Voltage and current waveforms at Bus B1, **c** Three phase power from renewables, and **d** FIS-based FDC outputs

three no-fault cases (NF) are the different operating conditions of RES with no fault on the transmission line. The accuracy and dependability of the proposed scheme are found to be 99.56% given in Table 9.

$$\text{Accuracy} = \frac{\text{total no. of cases detected correctly}}{\text{total no. of fault and no fault cases}} \times 100 \quad (3)$$

$$\text{Dependability} = \frac{\text{total no. of fault cases detected correctly}}{\text{total no. of actual fault cases}} \times 100 \quad (4)$$

The response or fault detection time of the proposed FIS-based protection module for different LG fault cases that are detailed in Table 2 is shown in Fig. 14. The *x*-axis represents the variation in fault location and the *y*-axis denotes fault detection time. The fault inception angle for the first and last three rows of figures are 0° and 90°, respectively. The fault resistance is 0.01 Ω (for 1st and 4th rows), 50 Ω (for 2nd and 5th), and 100 Ω (for 3rd and 6th rows). From Fig. 14, it can be observed that the different LG fault cases (AG faults in column-1, BG faults in column-2, and CG faults in column-3) are detected within half-cycle time. The fault detection time is also evaluated for the other fault cases in Table 2 and Table 10. It is noticed that the fault detection time is well within half-cycle time for all the LG, LLG, and LLL fault cases and one-cycle time for LL fault cases. The accuracy achieved and fault detection time of one-cycle time demonstrates the reliable operation of the proposed FIS protection module.

4.2 Performance evaluation of regression tree-based bagged ensemble learning module for fault location estimation

The effectiveness of the proposed fault location module is assessed for diverse fault cases considering varying fault locations using the percentage error metric defined in Eq. (5).

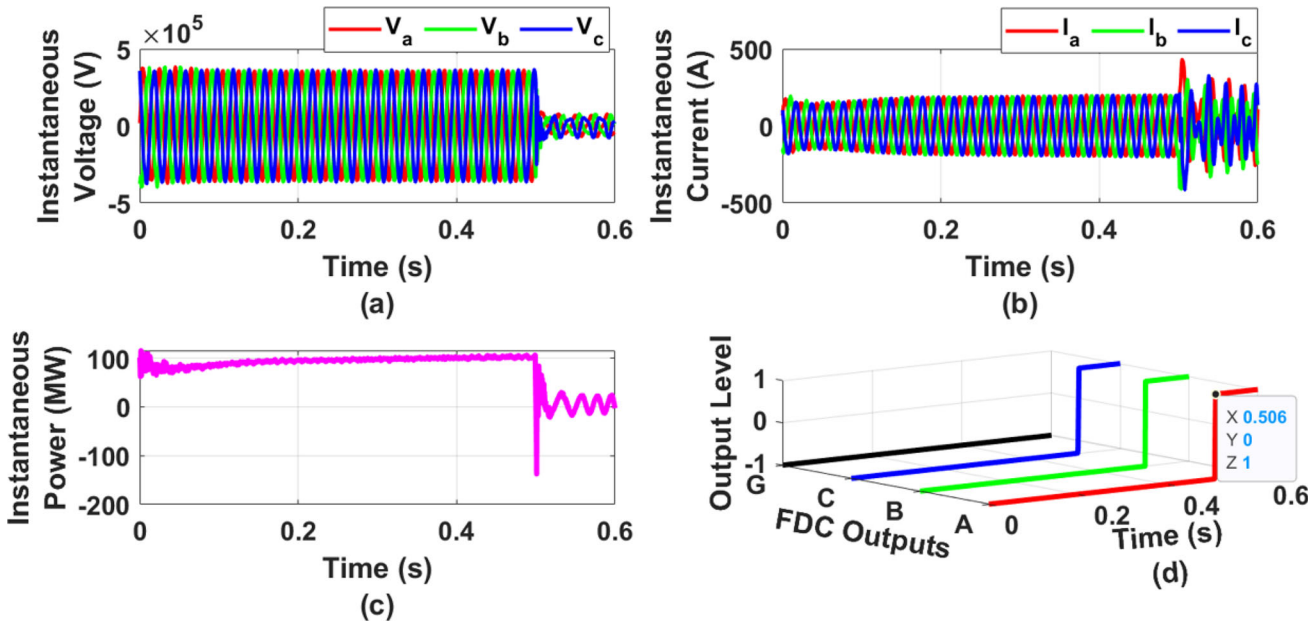

Fig. 13 ABC fault with $R_f = 30\ \Omega$, $\phi = 0°$ ($T_f = 0.5$ s), $L_f = 150$ km, solar irradiance = 1200 W/m^2, and wind speed = 20 m/s. **a** and **b** Voltage and current waveforms at Bus B1, **c** Three phase power from renewables, and **d** FDC outputs

Table 6 Performance results of the proposed FIS protection module for varying fault parameters

	Solar irradiance = 500 W/m^2 and wind speed = 8 m/s											
S. No.	Fault type	L_f (km)	R_f (Ω)	FIA (ϕ°) (T_f (s))	FIS-based FDC outputs				FDC time (ms)			
					A	*B*	*C*	*G*	*A*	*B*	*C*	*G*
1	AG	50 km	50 Ω	0° (0.5 s)	1	− 1	− 1	1	6 ms	–	–	1 ms
2	ABG	90 km	80 Ω	0° (0.5 s)	1	1	− 1	1	7 ms	4 ms	–	1 ms
3	AB	130 km	15 Ω	90° (0.505 s)	1	1	− 1	− 1	10 ms	8 ms	–	–
4	ABC	180 km	10 Ω	180° (0.51 s)	1	1	1	− 1	6 ms	3 ms	8 ms	–
5	BG	10 km	100 Ω	270° (0.515 s)	− 1	1	− 1	1	–	8 ms	–	1 ms
6	BCG	190 km	100 Ω	360° (0.52 s)	− 1	1	1	1	–	2 ms	9 ms	1 ms

Table 7 Performance results of the proposed FIS protection module for varying fault parameters

Solar irradiance = 1200 W/m^2 and wind speed = 20 m/s												
S. No.	Fault type	L_f (km)	R_f (Ω)	FIA (ϕ°) (T_f (s))	FIS-based FDC outputs				FDC time (ms)			
					A	B	C	G	A	B	C	G
1	ABC	150 km	30 Ω	0° (0.5 s)	1	1	1	− 1	6 ms	3 ms	8 ms	–
2	CAG	70 km	70 Ω	0° (0.5 s)	1	− 1	1	1	6 ms	–	8 ms	1 ms
3	CG	25 km	55 Ω	90° (0.505 s)	− 1	− 1	1	1	–	–	4 ms	1 ms
4	BC	160 km	25 Ω	180° (0.51 s)	− 1	1	1	− 1	–	2 ms	7 ms	–
5	ABG	197 km	100 Ω	270° (0.515 s)	1	1	− 1	1	9 ms	9 ms	–	2 ms
6	AG	3 km	0.01 Ω	360° (0.52 s)	1	− 1	− 1	1	3 ms	–	–	1 ms

Table 8 Confusion matrix for FDC

Detected faults		LG	LLG	LL	LLL	NF	Total
True faults	LG	1908	–	–	–	–	1908
	LLG	–	1880	–	28	–	1908
	LL	–	–	1908	–	–	1908
	LLL	–	–	–	636	–	636
	NF	–	–	–	–	3	3

Total no. of fault cases = 6363

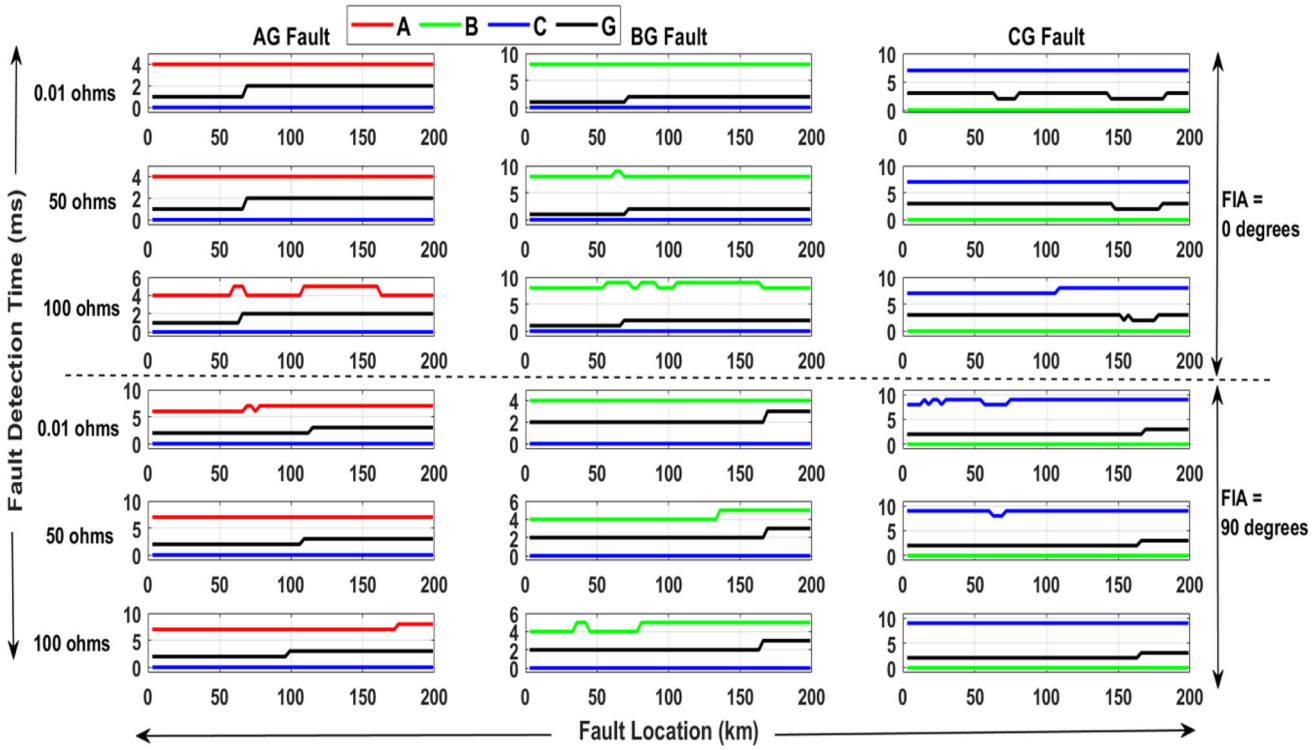

Fig. 14 Fault detection time of the proposed protection module with FIS for LG fault cases of Table 2

Table 9 Performance index of FIS based protection module

S. No.	Performance index
1	Accuracy = $\frac{6335}{6363} \times 100 = 99.56\%$
2	Dependability = $\frac{6332}{6360} \times 100 = 99.56\%$

This metric is the percentage error in estimated fault location that compares the estimated fault location (EFL) with the actual fault location (AFL), normalized by the total line *length* (L_T).

$$\%\text{Error in the estimated fault location } (\%E) = \frac{\text{EFL - AFL}}{L_T} \times 100 \quad (5)$$

An LG fault (AG) with $R_f = 0.01\ \Omega$ and $\phi = 0°$ is simulated at 9 km (AFL) from Bus B1. Figure 15 presents the output (L_e) of regression-based bagged ensemble learner towards the fault location estimation. When the system is healthy, the proposed bagged ensemble fault locator outputs 400 km. In case of a faulty condition, the proposed fault location module estimates fault location close to AFL, i.e. 8.551 km with a −0.2245% error in the EFL. Similarly, Figs. 16 and 17 depict the outputs of the fault location module for the LLG fault (ABG fault with $R_f = 90\ \Omega$ and $\phi = 0°$) and a triple line fault (ABC fault with $R_f = 0.01\ \Omega$ and $\phi = 0°$) simulated at 104 km (AFL) and 196 km (AFL), respectively. The EFL is found to be 108.13 km ($\%E = 2.065\%$) for the ABG fault and 193.10 km ($\%E = -1.45\%$) for the ABC fault with the proposed method of location estimation. In all the above-mentioned fault cases (AG, ABG, and ABC), the solar irradiance = 1000

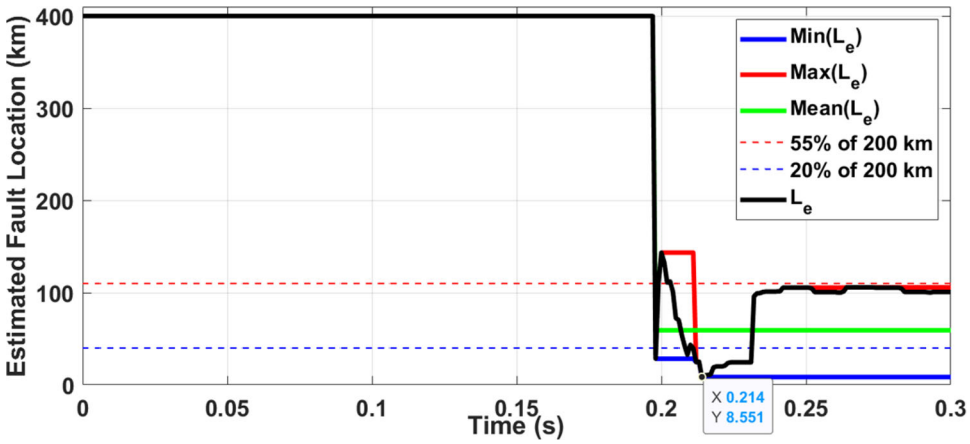

Fig. 15 Estimated fault location for AG fault with $R_f = 0.01\ \Omega$, $\phi = 0°$ and AFL = 9 km

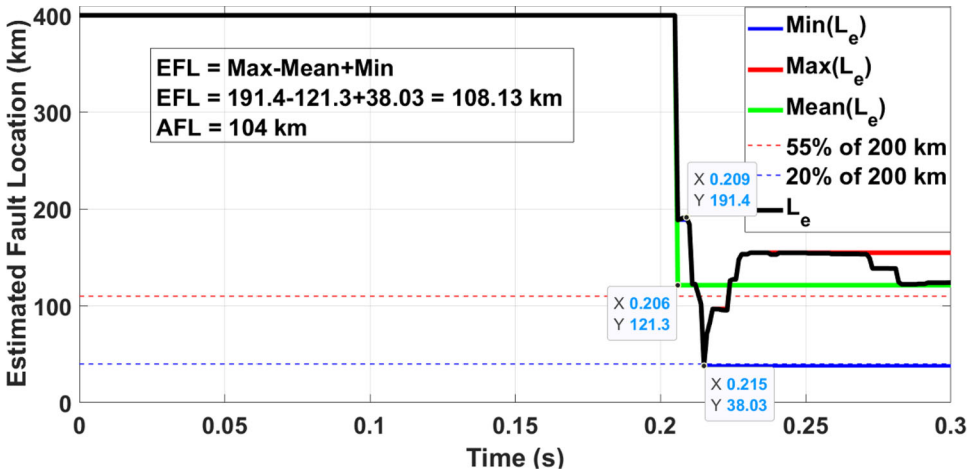

Fig. 16 Estimated fault location for ABG fault with $R_f = 90\ \Omega$, $\phi = 0°$ and AFL = 104 km

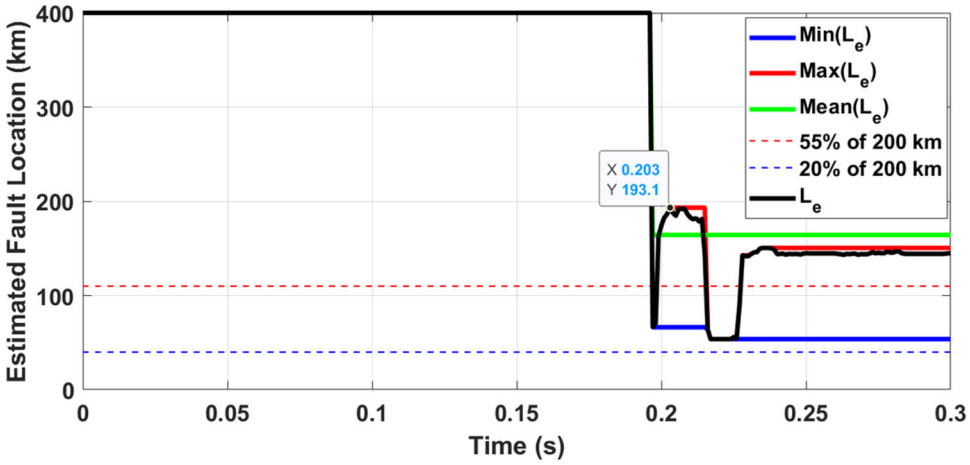

Fig. 17 Estimated fault location for ABC fault with $R_f = 0.01\ \Omega$, $\phi = 0°$ and AFL = 196 km

W/m^2 and wind speed = 15 m/s. To assess the effectiveness of the proposed fault location module, a testing data set is created by simulating different types of faults and Table 10 gives the details of fault parameters considered that counts for 2400 different fault cases. Figure 18 presents the scatter plot of percentage error in the estimated fault location for different faults mentioned in Table 10. It is noticed that the $\%E$ lies in the band of $\pm 5\%$ with the proposed method. Table 11 presents the results of estimated fault location for different faults. Further, to assess the reliability of the fault location module, Chi-square error analysis is performed on 400 EFL errors that are obtained by randomly simulating the faults at different locations along the transmission line. Table 12 presents the Chi-square test for reliability analysis of the

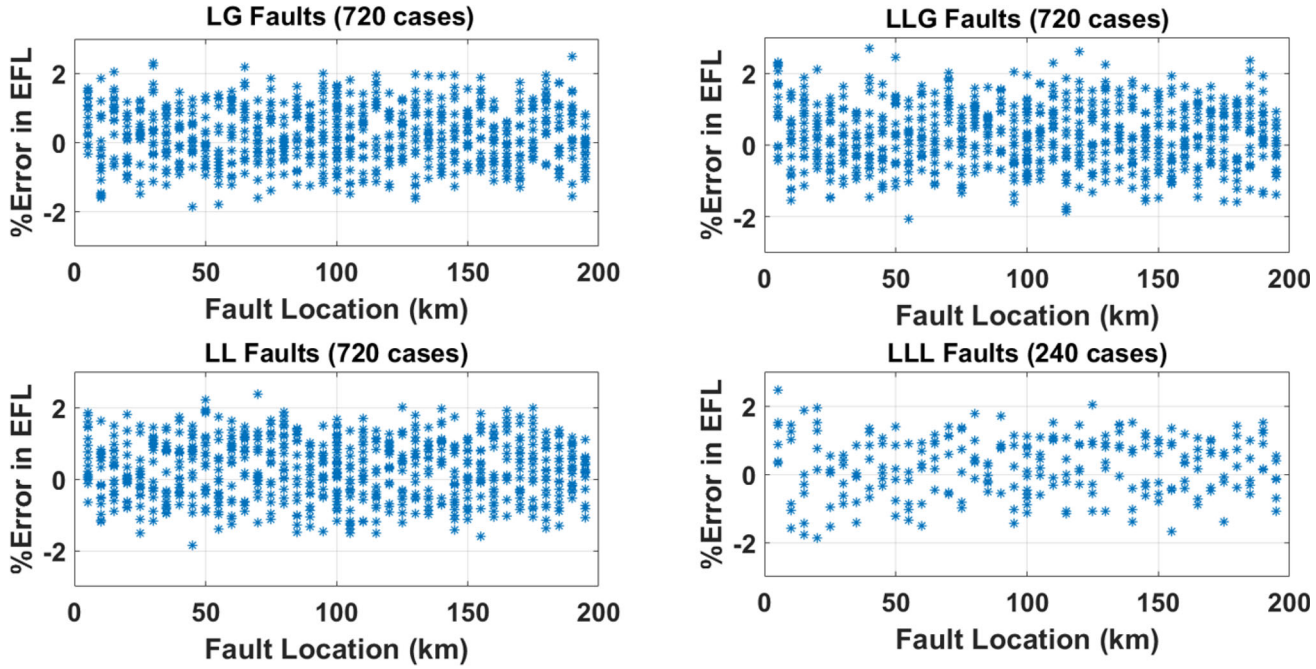

Fig. 18 Percentage error in estimated fault location for all fault cases of Table 10

proposed fault location estimation method. The low difference between the observed and expected number of errors showcases the efficacy of the proposed method and the Chi-square value (D^2) falls in the 5% band of significance level [34].

4.3 Comparison of the proposed scheme of protection

A comparison of the proposed scheme of protection is discussed in this section in terms of protection and feature extraction techniques, protection tasks implemented, type of RES integrated, and FDC accuracy. Table 13 provides a comparison of different protection schemes with the proposed method. All the protection methods mentioned in Table 13 are training based artificial intelligent methods for the detection and classification of faults except the proposed one. The training-based methods require large sets of training data considering different operating conditions to train the models for achieving high performance and accuracy of the trained models in the protection tasks. The proposed scheme is implemented with the fuzzy inference concept for fault detection and classification that do not require any training of the module. Further, the FDC accuracy is comparably high with other training-based techniques.

5 Conclusion

In this paper, an FIS-based protection module for the detection/classification of short circuit faults and a bagged ensemble learning approach with regression trees for approximating actual fault location has been proposed for the transmission line connected to RES (solar PV and DFIG-based wind power). The proposed protection modules utilize only the DFT processed three-phase voltage information of a single bus (i.e. connected to RES). Hence, the communication link is not required and no communication latency. The proposed FIS based protection module effectively detects the fault occurrence and classifies the different short circuit fault types within one cycle time (20 ms) following the fault inception even for varying fault parameters under different operating conditions of RES. This showcases that the proposed detection/classification scheme is passive/robust to fault parameter variations and RES power intermittences. Further, the performance index indicates the efficacy of the FDC scheme with an accuracy of 99.56% calculated with the help of confusion matrix. The proposed fault location module with bagged ensemble of regression trees successfully predicts the actual fault location with minimal error. The percentage error in the estimated fault location is within ±5% error band even for various faults with varying fault

Table 10 Fault parameters considered in the testing data set

S. No.	Fault parameter	Variations
1	Fault resistance (Ω)	30 Ω, 60 Ω, and 90 Ω (3 no.)
2	Fault inception angle (°)	45° and 180° (2 no.)
3	Fault location (km)	5 km, 10 km, 15 km, …, 190 km, and 195 km (40 no.)
4	Fault types	10 (ABC, AB, BC, CA, ABG, BCG, CAG, AG, BG, and CG)
Therefore, the total no. of fault cases considered = 3*2*40*10 = 2400		

Table 11 Performance of the proposed bagged ensemble learner module for different faults

S. No.	Fault type	AFL (km)	R_f (Ω)	FIA (ϕ°)	EFL (km)	% Error
1	AG	5 km	50 Ω	0°	5.38 km	0.19
2	ABG	70 km	0.01 Ω	0°	71.74 km	0.87
3	AB	120 km	20 Ω	0°	116.45 km	− 1.76
4	ABC	190 km	0.01 Ω	0°	191.27 km	0.64
5	BG	50 km	60 Ω	90°	45.66 km	− 2.17
6	BCG	100 km	100 Ω	90°	99.31 km	− 0.35
7	BC	150 km	10 Ω	90°	144.73 km	− 2.64
8	ABC	30 km	15 Ω	90°	30.87 km	0.44
9	CG	130 km	100 Ω	270°	127.65 km	− 1.18
10	CAG	80 km	90 Ω	270°	79.48 km	− 0.26
11	CA	195 km	25 Ω	270°	193.19 km	− 0.91
12	ABC	197 km	10 Ω	270°	193.35 km	− 1.825

Table 12 Chi-square test for fault location estimation reliability analysis

Interval number *(i)*	% Error interval	No. of observed errors (N_{oi})	No. of expected errors (N_{ei})	$\frac{(N_{oi}-N_{ei})^2}{N_{ei}}$
1	− 4.5 to − 3.5	7	5	0.8
2	− 3.5 to − 2.5	22	19	0.4737
3	− 2.5 to − 1.5	39	46	1.0652
4	− 1.5 to − 0.5	78	82	0.1951
5	− 0.5 to 0.5	104	101	0.0891
6	0.5 to 1.5	86	83	0.1084
7	1.5 to 2.5	44	46	0.087
8	2.5 to 3.5	20	18	0.2222
$D^2 = \sum_{i=1}^{8} \frac{(N_{oi}-N_{ei})^2}{N_{ei}} = 3.0407$				

parameters demonstrating the adaptability to diverse fault scenarios. Further, the reliability of the fault location estimation module is confirmed through the statistical analysis with the Chi-square test ($D^2 = 3.0407$) on location errors falling in the 5% band of the significance level. The proposed approach exemplifies the potential of combining fuzzy logic, ensemble learning, and signal processing techniques for developing intelligent protection systems adaptable to modern power grids.

Table 13 Comparison with other protection schemes

Comparison term	References						
	[18]	[19]	[35]	[36]	[37]	[38]	Proposed
Protection technique based on	SVM	ANN	SVM and GPR	Rotation forest	Decision tree and SVM	Random forest	FIS and regression-based bagged ensemble learner
Signal pre-processing or features utilized	Transient motoring index of currents	MODWT; energy of detail coefficients of voltage and current	RMS of voltages and currents	DWT; standard deviation of approximate coefficients of voltage and current	DFT; amplitude and phase angle of voltage and current phasors	Positive sequence currents and empirical mode decomposition of grid side currents	DFT; magnitudes zero-sequence and fundamental components of phase voltages
Protection tasks	FDC	FD of symmetrical faults only	FDC and FLE	FDC	FDC and FLE	FDC and FLE	FDC and FLE
FDC accuracy	99.84%	98.40%	99.50%	99.43%	97.9%	99.95%	99.56%
FDC time	10 ms	–	20 ms	16.67 ms	–	8 ms	20 ms
PV and/or wind power integration	Wind power	Wind power	– (DGs)	PV and wind power	Wind power	Wind power	PV and wind power

FD Fault detection *FDC* Fault detection and classification, and *FLE* Fault location estimation

Authors contribution Gotte Vikram Raju provided conceptualization, methodology, software, investigation, and writing—original draft preparation. Nandiraju Venakata Srikanth performed supervision, conceptualization, validation, and writing—reviewing and editing.

Funding Not Applicable.

Data availability There are no new data generated in this work. Whatever data used are available openly and cited properly. Moreover, the new findings in this work are kept openly.

Declarations

Conflict of interest The authors declare that they have no competing interests.

Appendix

See Tables 14, 15 and 16

Table 14 Transmission line parameters

Data of transmission line parameters (200 km line length)		
Parameter	Positive and negative	Zero
Resistance (Ω/km)	0.0275	0.275
Inductance (H/km)	1.002e–03	3.268e–03
Capacitance (F/km)	13e–09	8.5e–09

Table 15 Solar PV data

PV Data		Module Specifications	
Rated power	50 MW (1 MW units)	PV module type	1Soltech 1STH-350-WH
L_B	1.7 mH	Rated power	349.59 W
Switching frequency	2.1 kHz	Open circuit voltage (V_{oc})	51.5 V
R_{filter1}	0.0015 pu	Short circuit current (I_{sc})	9.4 A
L_{filter1}	0.15 pu	Voltage at max. power point	43 V
Q_{filter1}	0.1 pu	Current at max. power point	8.13 A
V_{dc1}	1200 V	Temperature coefficient of V_{oc}	− 0.36%/°C
DC link capacitor	16.45 mF	Temperature coefficient of I_{sc}	0.09%/°C
Voltage regulator (PI-1)	$K_p = 7$ and $K_i = 800$		
Current regulator (PI-2)	$K_p = 0.3$ and $K_i = 20$		

Table 16 Wind farm data

DFIG-based wind farm data			
Rated power of wind farm	50 MW	No. of pole pairs (p)	3
Rated power of wind turbine	1.5 MW	DC link voltage (V_{dc2})	1150 V
Wind turbine inertia constant (H_{t})	4.32 s	R_{filter2}	0.003 pu
Nominal power generator	1.5/0.9 MW	L_{filter2}	0.3 pu
Inertia constant (H_{g})	0.685 s	Q_{filter2}	0.08 pu
Nominal stator voltage	575 V	Switching frequency (GSC)	2.7 kHz
Nominal rotor voltage	1975 V	PI-3 (GSC)	$K_p = 8$ and $K_i = 400$
Stator resistance (R_{s})	0.023 pu	PI-4 (GSC)	$K_p = 0.83$ and $K_i = 5$
Rotor resistance (R_{r})	0.016 pu	Switching frequency (RSC)	1.62 kHz
Stator inductance (L_{s})	0.18 pu	Voltage regulator (RSC)	$K_p = 5$ and $K_i = 20$
Rotor inductance (L_{r})	0.16 pu	PI-5 (RSC)	$K_p = 0.6$ and $K_i = 8$
Magnetizing inductance (L_{m})	2.9 pu		

References

1. Hooshyar A, Iravani R (2017) Microgrid protection. Proc IEEE 105:1332–1353. https://doi.org/10.1109/JPROC.2017.2669342
2. Quispe JC, Orduña E (2022) Transmission line protection challenges influenced by inverter-based resources: a review. Prot Control Mod Power Syst 7:1–17. https://doi.org/10.1186/s41601-022-00249-8
3. Li X, Lu Y (2023) Pilot protection of lines emanating from DFIG-based wind farms during balanced faults. Int J Electr Power Energy Syst. https://doi.org/10.1016/j.ijepes.2023.109186
4. Chakeri V, Seyedi H, Tarafdar Hagh M (2021) A new approach to transmission line pilot protection in the presence of inverter-interfaced distributed generators. IEEE Syst J 15:5383–5392. https://doi.org/10.1109/JSYST.2020.3041203
5. Hu Z, Li B, Zheng Y, Wu T, He J, Yao B, Sheng Y, Dai W, Li X (2023) Fast distance protection scheme for wind farm transmission lines considering R-L and bergeron models. J Mod Power Syst Clean Energy 11:840–852. https://doi.org/10.35833/MPCE.2021.000423
6. Ma K, Hoidalen HK, Chen Z, Bak CL (2023) Improved zone 1 topline tilting scheme for polygonal distance protection in the outgoing line of type-4 wind parks. CSEE J Power Energy Syst 9:172–184. https://doi.org/10.17775/CSEEJPES.2021.07870
7. Paladhi S, Pradhan AK (2021) Adaptive distance protection for lines connecting converter-interfaced renewable plants, IEEE. J Emerg Sel Top Power Electron 9:7088–7098. https://doi.org/10.1109/JESTPE.2020.3000276
8. Saber A, Shaaban MF, Zeineldin HH (2022) A new differential protection algorithm for transmission lines connected to large-scale wind farms. Int J Electr Power Energy Syst 141:108220. https://doi.org/10.1016/j.ijepes.2022.108220

9. Aboshady FM, Saber A, Khera F, Zobaa AF (2023) High frequency directional-based protection scheme for transmission lines emanating from large scale wind farms. Electr Power Syst Res 225:109904. https://doi.org/10.1016/j.epsr.2023.109904
10. Li B, Liu J, Wang X, Zhao L (2018) Fault studies and distance protection of transmission lines connected to DFIG-Based wind farms. Appl Sci. https://doi.org/10.3390/app8040562
11. Li B, Sheng Y, He J, Li Y, Xie Z, Cao Y (2023) Improved distance protection for wind farm transmission line based on dynamic frequency estimation. Int J Electr Power Energy Syst. https://doi.org/10.1016/j.ijepes.2023.109382
12. Ghorbani A, Mehrjerdi H (2023) Distance protection with fault resistance compensation for lines connected to PV plant. Int J Electr Power Energy Syst 148:108976. https://doi.org/10.1016/j.ijepes.2023.108976
13. Chowdhury A, Paladhi S, Pradhan AK (2023) Local positive sequence component based protection of series compensated parallel lines connecting solar photovoltaic plants. Electr Power Syst Res 225:109811. https://doi.org/10.1016/j.epsr.2023.109811
14. Singh S, Nayak PK, Sarangi S, Biswas S (2022) Improved protection scheme for high voltage transmission lines connecting large-scale solar PV plants, 2022 22nd Natl. Power Syst Conf NPSC 2022:118–123. https://doi.org/10.1109/NPSC57038.2022.10069457
15. Liang Y, Xu G, Zha W, Wang C (2019) Adaptability analysis of fault component distance protection on transmission lines connected to photovoltaic power stations. Energies 12:1578. https://doi.org/10.3390/en12081578
16. Yoldas YB, Yumurtacı R (2023) Improvement of distance protection with SVM on PV-Fed transmission lines in infeed conditions. Energies 16:1–18. https://doi.org/10.3390/en16062587
17. Noureldeen O, Hamdan I, Hassanin B (2019) Design of advanced artificial intelligence protection technique based on low voltage ride-through grid code for large-scale wind farm generators: a case study in Egypt. SN Appl Sci 1:1–19. https://doi.org/10.1007/s42452-019-0538-9
18. Mohanty SK, Nayak PK, Bera PK, Alhelou HH (2023) An enhanced protective relaying scheme for TCSC compensated line connecting DFIG-Based wind farm. IEEE Trans Ind Inf. https://doi.org/10.1109/TII.2023.3306575
19. Alrashdan AA, Feilat EA, Haj-Ahmed MA, Protection of transmission lines emanating from DFIG-based wind farms during symmetrical faults, In: Conf. Rec. - IAS Annu. Meet. (IEEE Ind. Appl. Soc. 2021-Octob (2021) 1–6. https://doi.org/10.1109/IAS48185.2021.9677091.
20. Biswas S, Nayak PK, Panigrahi BK, Pradhan G (2023) An intelligent fault detection and classification technique based on variational mode decomposition-CNN for transmission lines installed with UPFC and wind farm. Electr Power Syst Res 223:109526. https://doi.org/10.1016/j.epsr.2023.109526
21. Mohanty SK, Santra SB, Siano P (2023) Faulty phase identification and ground detection in TCSC compensated lines integrated with wind farms. Int J Electr Power Energy Syst 153:109383. https://doi.org/10.1016/j.ijepes.2023.109383
22. Prasad CD, Biswal M (2020) Swarm intelligence-based differential protection scheme for wind integrated transmission system. Comput Electr Eng 86:106709. https://doi.org/10.1016/j.compeleceng.2020.106709
23. Prasad CD, Biswal M, Abdelaziz AY (2020) Adaptive differential protection scheme for wind farm integrated power network. Electr Power Syst Res 187:106452. https://doi.org/10.1016/j.epsr.2020.106452
24. Tazay AF, Ibrahim AMA, Noureldeen O, Hamdan I (2020) Modeling, control, and performance evaluation of grid-tied hybrid pv/wind power generation system: case study of gabel el-zeit region, egypt. IEEE Access 8:96528–96542. https://doi.org/10.1109/ACCESS.2020.2993919
25. Wang L, Vo QS, Prokhorov AV (2018) Stability improvement of a multimachine power system connected with a large-scale hybrid wind-photovoltaic farm using a supercapacitor. IEEE Trans Ind Appl 54:50–60. https://doi.org/10.1109/TIA.2017.2751004
26. Bhide SR (2014) Digital power system protection. PHI Learning Private Limited, Delhi
27. Timothy RJ (2010) Fuzzy logic with engineering applications, 3rd edn. Wiley, Chichester
28. Breiman L (1996) Bagging predictors. Mach Learn 24:123–140. https://doi.org/10.1023/A:1018054314350
29. Polikar R (2006) Ensemble based systems in decision making. IEEE Circuits Syst Mag 6:21–44. https://doi.org/10.1109/MCAS.2006.1688199
30. MATLAB, Tree Baggers Document, (n.d.). https://in.mathworks.com/help/stats/treebagger.html.
31. Breiman L, Friedman JH, Olshen RA, Stone CJ (1998) Classification and regression trees, 1st edn. CRC Press, Baco Raton
32. Grabczewski K (2014) Meta-learning in decision tree induction. Springer, New York. https://doi.org/10.1007/978-3-319-00960-5
33. Loh W-Y (2010) Classification and regression trees, Wiley interdiscip. Rev. Data Min. Knowl. Discov. 1:14–23. https://doi.org/10.1002/widm.8
34. Koley E, Shukla SK, Ghosh S, Mohanta DK (2017) Protection scheme for power transmission lines based on SVM and ANN considering the presence of non-linear loads. IET Gener Transm Distrib 11:2333–2341. https://doi.org/10.1049/iet-gtd.2016.1802
35. Srivastava A, Parida SK (2022) A robust fault detection and location prediction module using support vector machine and gaussian process regression for AC microgrid. IEEE Trans Ind Appl 58:930–939. https://doi.org/10.1109/TIA.2021.3129982
36. Manohar M, Koley E, Ghosh S (2020) Stochastic weather modeling-based protection scheme for hybrid PV-wind system with immunity against solar irradiance and wind speed. IEEE Syst J 14:3430–3439. https://doi.org/10.1109/JSYST.2020.2964990
37. Uddin MN, Rezaei N, Arifin MS (2023) Hybrid machine learning-based intelligent distance protection and control schemes with fault and zonal classification capabilities for grid- connected wind farms. IEEE Trans Ind Appl 59:7328–7340. https://doi.org/10.1109/TIA.2023.3302836
38. Biswas S, Nayak PK (2021) A new approach for protecting TCSC compensated transmission lines connected to DFIG-based wind farm. IEEE Trans Ind Inf 17:5282–5291. https://doi.org/10.1109/TII.2020.3029201